ChemComm

Accepted Manuscript

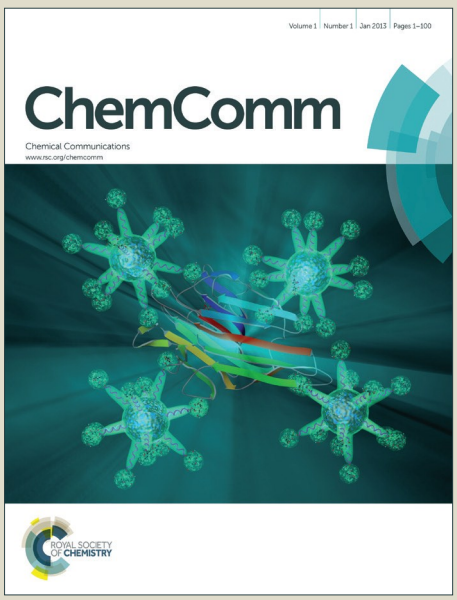

ROYAL SOCIETY OF CHEMISTRY

www.rsc.org/chemcomm

Journal Name

COMMUNICATION

Simple synthesis of urchin-like Pt-Ni bimetallic nanostructures as enhanced electrocatalysts for oxygen reduction reaction †

Received 00th January 20xx,
Accepted 00th January 20xx

DOI: 10.1039/x0xx00000x

www.rsc.org/

Kwang-Hyun Choi,‡[ab] Youngjin Jang,‡[ab‖] Dong Young Chung,‡[ab] Pilseon Seo,[ab] Samuel Woojoo Jun,[ab] Ji Eun Lee,[ab⊥] Myoung Hwan Oh,[ab] Mohammadreza Shokouhimehr,[ab] Namgee Jung,[c] Sung Jong Yoo,[d] Yung-Eun Sung*[ab] and Taeghwan Hyeon*[ab]

The synthesis of urchin-like Pt-Ni bimetallic nanostructures are achieved by a controlled one-pot synthesis. Pt-Ni nanostructures have superior oxygen reduction reaction activities in both with and without specific anion adsorption electrolytes due to the geometric and alloying effect.

Platinum group metal (PGM)-based materials have been a dominant class of electrocatalysts for efficient oxygen reduction reaction (ORR) of proton exchange membrane fuel cell (PEMFC).[1,2] As the scarcity and high cost of Pt metal hinder the commercialization of the fuel cells, many of the fuel cell researchers have focused on the development of the catalysts with the less amount of Pt and the higher activity.[3] There have been so far several synthetic approaches reported to accomplish this goal by controlling the shape and composition of the Pt-based nanocatalysts.[4,5] Since Stamenkovic *et al.* demonstrated the enhanced performance of Pt-Ni bimetallic materials in ORR,[5a] a number of synthetic methods for the preparation of Pt-Ni bimetallic nanoparticles with various shapes including octahedron,[5b-f] cuboctahedron,[5f-g] truncated octahedron,[5h] cube,[5c-d] and icosahedron[5i] have been reported. Especially, among the various shapes, the dendritic nanostructures have attracted much attention for their enhanced electrocatalytic performance.[6] This is attributed to their large specific surface area and rough surface with more edges and kinks compared to the nanoparticles with convex shapes.[5g,6b] However, despite of the recent progress in the synthesis of Pt-based nanomaterials, the synthesis of shape and composition-controlled bimetallic nanoparticles and the optimization for the electrocatalytic performance are still remained elusive. In this communication, we report the facile one-pot synthesis of the urchin-like Pt-Ni nanostructures with the Pt-to-Ni composition adjustable in the range from 1:1 to 3:1. The urchin-like Pt-Ni nanostructures with different compositions are applied to the oxygen reduction electrocatalyst. Overall, the urchin-like Pt-Ni nanostructures exhibit better electrocatalytic performance compared with the commercial Pt catalysts due to alloying effect. In addition, we found that the urchin-like morphology of our nanostructures is advantageous with the low susceptibility towards specific anion adsorption, such as H_2SO_4, which is attributed to their shape control process.

Urchin-like Pt-Ni bimetallic nanostructures are synthesized by a simple heat-up process.[7] A reaction solution is prepared by dissolving $Pt(acac)_2$, $Ni(acac)_2$, 1-hexadecylamine (HDA), and 1-adamantanecarboxylic acid (ACA) in benzyl ether and heated up to 240 °C at the rate of 4 °C/min and then aged for 30 min at that temperature. The composition of the bimetallic nanostructures is controlled by changing the amount of the Ni precursor in the solution while fixing that of Pt. In Fig. 2a, transmission electron microscopy (TEM) images of Pt-Ni nanostructures synthesized with different molar ratios of Pt and Ni precursors are shown. For the precursor feeding ratios of Pt:Ni = 1:1, 2:1, and 3:1, the compositions of the obtained nanostructures are measured as $Pt_{51.5}Ni_{48.5}$, $Pt_{66.7}Ni_{33.3}$, and $Pt_{75.1}Ni_{24.9}$, respectively, by inductively coupled plasma atomic emission spectroscopy (ICP-AES). Such good match between the feeding ratio and the composition of the nanostructures demonstrates simple and effective composition control of this

[a] Center for Nanoparticle Research, Institute for Basic Science (IBS), Seoul, 151-742, Korea. Fax: (+82) 2-886-8457; Tel: (+82) 2-880-7150; E-mail: ysung@snu.ac.kr, thyeon@snu.ac.kr
[b] School of Chemical and Biological Engineering, Seoul National University, Seoul, 151-742, Korea.
[c] Department of Energy Science and Technology, Graduate School of Energy Science and Technology (GEST), Chungnam National University, Daejeon, 305-764, Republic of Korea
[d] Fuel Cell Research Center, Korea Institute of Science and Technology (KIST), Seoul, 136-791, Korea

† Electronic Supplementary Information (ESI) available: [Details of synthesis and characterization, additional TEM, XRD, ICP, XANES, and EXAFS data, cyclic voltammograms of Pt-Ni nanostructures and the commercial Pt catalyst.]. See DOI: 10.1039/b000000x/

‡ These authors contributed equally to this work.

‖ Current address: Schulich Faculty of Chemistry, Russell Berrie Nanotechnology Institute, Technion, Haifa, 32000, Israel

⊥ Current address: Creative Research Center, Creative and Fundamental Research Division, Korea Electrotechnology Research Institute (KERI), Changwon, Gyeongsangnam-do, 641-120, Korea

synthesis. Energy-filtered TEM (EFTEM) images in Fig. 1b shows homogeneous distribution of both Pt and Ni atoms

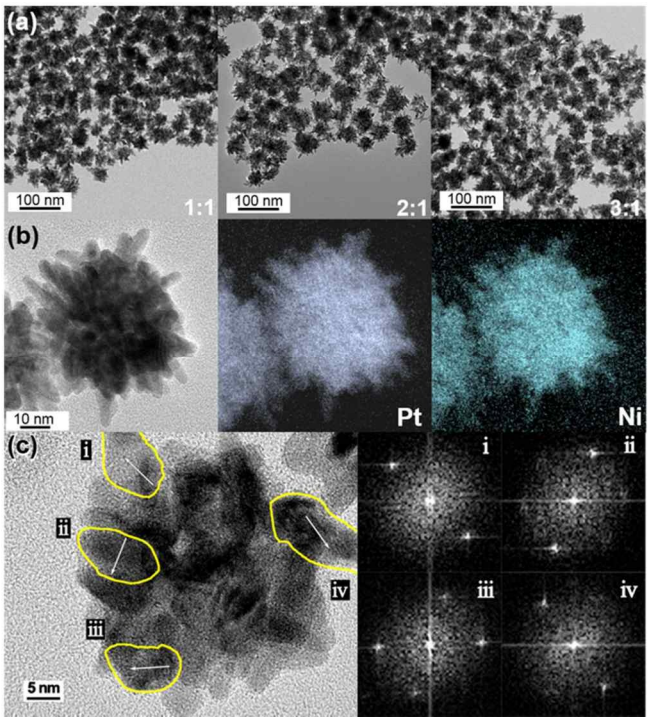

Fig. 1 (a) TEM images of PtxNi nanostructures (Pt:Ni), (b) EF-TEM image of Pt_2Ni and element mapping images, and (c) magnified TEM images and FFT patterns.

within a nanostructure. X-ray diffraction (XRD) measurement confirms face-centred cubic (fcc) structure of the nanostructures (Fig. S1, ESI†). The position of the diffraction peaks are monotonically shifted to the higher 2θ values as the composition of Ni increases, indicating the lattice contraction due to the smaller atomic radius of Ni compared to Pt. No characteristic peaks from either nickel or nickel oxide species are observed. In Fig. 1c, a high-resolution TEM image of an urchin-like nanostructure is shown. This structure consists of a number of the smaller nanoplatelets fused together. As indicated with arrows in the figure, the crystallographic orientations of the platelets consisting a single nanostructure are random. This observation strongly suggests that the urchin-like nanostructure is not a result of branched growth from the seed core, in which case the crystal lattices in the core and the branches are coherent, as reported previously (Ref. 6a).

To study the process of Pt-Ni nanostructure formation, we analysed a series of aliquots sampled from the solution with the Pt:Ni feeding ratio of 2:1 at different points of time during the synthesis. TEM analysis shows that irregular-shaped nanoparticles appear in the solution at 220 °C and grow further into urchin-like structures during aging at 240 °C (Fig. S2, ESI†). In the meantime, the composition of the nanoparticles separated from the aliquots is changed from only Pt at 220 °C to $Pt_{2.06}Ni$ at the end of the reaction (Table S1, ESI†). X-ray absorption near edge structure (XANES) data at Pt L_{III} edge and Ni K edge show that reduction of both Pt^{2+} and Ni^{2+} occurs simultaneously during heating from 230 °C to 15 min aging at 240 °C (Fig. S3, ESI†). These observations suggest a reaction model that a small portion of Pt^{2+} cations are reduced by HDA under heating first ($Pt^{2+} + 2RNH_2 \rightarrow Pt^0 + 2RNH_2^{+\bullet}$)[8a] and the the pre-formed Pt clusters and nanoparticles catalyse the reduction of Ni^{2+} and the rest of Pt^{2+}.[8b-c] At the surface of the metal, transition metal cations can be reduced at the less negative potentials compared to those without Pt, which is known as underpotential deposition.[8c-d] Actually, in a control experiment using only Ni precursor in the synthesis, no particles are formed, conforming that the presence of Pt is necessary for the reduction of Ni^{2+} in the current reaction condition. In addition, due to the large difference in the standard reduction potentials of Ni^{2+} and Pt^{2+} (-0.25 V and 1.188 V vs. SHE, respectively), galvanic replacement can take place between Ni atoms at the surface of the nanostructures and Pt^{2+} in the solution ($Ni_{(s)} + Pt^{2+} \rightarrow Ni^{2+} + Pt_{(s)}$). As a result, the presence of Ni^{2+}/Ni can affect the overall reduction reaction kinetics via underpotential deposition and galvanic replacement.

The effect of Ni^{2+}/Ni on the reaction kinetics can be deduced from the shape evolution of urchin-like nanostructures. Firstly, in a synthesis using only Pt precursor, truncated Pt nanoparticles with the size of 30 nm are obtained (Fig. S4, ESI†). This proves the critical role of the Ni precursor in the shape evolution. In general, PGM-based nanoparticles with ill-defined shape and high surface area, such as dendritic and urchin-like structures, are formed when the reduction rate is very high because those shapes are far from thermodynamic equilibrium.[9] If the reduction is slow, the nanoparticles are in quasi-equilibrium with the solution and tend to have more stable shapes exposing the low energy facet, for example, octahedron with (111) facet for fcc structure. Actually, when the reaction temperature is raised to 260 °C, extensive ripening takes place for the urchin-like nanostructures which turns them to spherical nanoparticles with broad size distribution (Fig. S5, ESI†). Therefore, it seems that the presence of Ni^{2+}/Ni accelerates the overall reduction rate so that thermodynamically unstable urchin-like shapes can be formed that expose higher energy facets.

The electrocatalytic activity of the urchin-like Pt-Ni nanostructures with different compositions is evaluated by cyclic voltammetry (CV) and polarization curve measurements (Fig. 2a and Fig. S6, ESI†). Among the samples, Pt_2Ni nanostructures show the best mass activity, which is 12.2 times higher than that of commercial Pt/C nanoparticle (Table 1). Overall, the urchin-like nanostructures have the higher specific activity than commercial Pt/C. (Pt_2Ni nanostructures show 15.5 times higher specific activity than that of commercial Pt/C nanoparticle.) The enhanced ORR activity is attributed to the electronic perturbation from alloying that can adjust the adsorption energy of oxygen species on Pt.[10] This adjustment can lower the strong adsorption energy of OH, which blocks the active surface area. In our experiment, this effect is proved by positive peak potential shift of Pt-OH reduction in CV (Fig. S6, ESI†). The Pt_2Ni nanostructures show the lower white line intensity of Pt L_{III} XANES spectrum than that of commercial Pt catalyst (Fig. S7). This indicates the

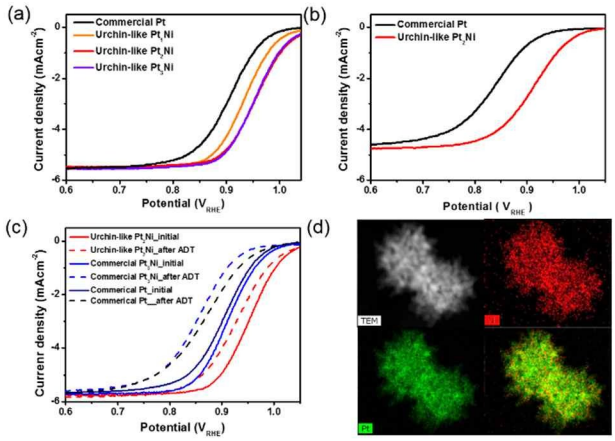

Fig. 2 (a) polarization curves of the Pt_xNi nanostructures with three different compositions (x=1, 2, and 3) and the reference commercial Pt catalyst in $HClO_4$ electrolyte (b) polarization curves in H_2SO_4 electrolytes (c) long-term durability results and (d) HAADF-STEM and EDS mapping images of urchin-like Pt_2Ni nanostructures after ADT.

higher electron population in the 5d band, which results in the lower adsorption energy.

As mentioned above, it is conjectured that the higher energy facets are exposed at the surface of our urchin-like nanostructures, unlike thermodynamically stable shapes exposing mainly (111). It is well known that for Pt-based catalysts (111) surface has the highest ORR activity than the other facets.[5a,5c,11] However, on the other hand, in commercial hydrogen fuel cell operation, the interaction between the catalyst and the sulfonic acid groups in Nafion® can poison the catalyst via specific anion adsorption[3a,12] and this adverse effect is the most significant on (111).[11] Therefore, it is important for the catalyst to balance the activity with the resistivity towards specific anion adsorption. The surface orientation of the urchin-like Pt_2Ni nanostructures is studied by CVs in H_2SO_4 solution under Ar and the result is compared with that of commercial Pt catalyst (Fig. S8, ESI†). The butterfly peak around 0.5 V vs RHE from commercial Pt is correlated with the specific anion adsorption on Pt(111).[4a,13] In contrast, only very weak signal is observed in the same region from the urchin-like Pt_2Ni nanostructures. The CV curve in hydrogen underpotential deposition (H_{upd}) region (0.05 <V< 0.3, V vs. RHE) shows that (100) planes, rather than (111), are dominant on the surface of the urchin-like Pt_2Ni nanostructures, which confirms our expectation based on the thermodynamic consideration on the formation process. Due to the (100) dominant-surface, the specific activity of the Pt_2Ni nanostructures from the ORR measurement in H_2SO_4 electrolyte is 20.7-fold higher than that of commercial Pt/C nanoparticle (Pt_2Ni: 0.456 mA/cm^2_{Pt} and Pt/C: 0.022 mA/cm^2_{Pt}), as shown in Fig. 2b. This result demonstrates that our bimetallic PtNi nanostructures have good tolerance for specific anion adsorption while maintaining high activity.

The long-term stability study is conducted through accelerated durability test (ADT) with United States Department of Energy protocol. To separate the shape and

Table 1. Summary of electrochemical results in $HClO_4$ electrolyte

	Mass activity (A/mg_{Pt})	Specific activity (mA/cm^2_{Pt})	ECSA (m^2/g)
Pt/C (commercial)	0.13	0.19	68.4
Pt_1Ni	0.75	1.21	62.0
Pt_2Ni	1.59	2.94	54.1
Pt_3Ni	1.53	2.90	52.8

composition effects on the long-term stability, we also teste[d] commercial Pt_3Ni/C nanoparticles with spherical shape (Fig. 2[c] and Table S2). After 10,000 cycles, Pt_2Ni nanostructures sho[w] the minimum activity loss among the samples. Scanning transmission electron microscopy (STEM) data show that the morphology of the nanostructures is retained after ADT (Fig. 2[d]). This observation is also consistent with the previous reports that branched and dendritic nanoparticles tend to be mo[re] resistive towards coalescence during cycles than the spherical shapes.[14] This effect can be explained in terms of the structu[ral] factor. Unlike nanoparticles of well-defined shapes such [as] sphere and polyhedrons, contact of two urchin-like nanostructures leads to the formation of complex interface structure due to their irregular shape and randor[m] crystallographic orientations of the subdomains, as shown in Fig. 1c, which makes the coalescence energetically less favoure[d]. We found that the surface of our nanostructures is Pt-rich eve[n] before cycling. X-ray photoelectron spectroscopy (XPS) data ([Fig.] S9 and S10) show low Ni 2p signal intensity compared to that of Pt 4f after synthesis and no Ni signal after the deposition of th[e] nanostructures onto Vulcan XC-72R (Fig. S11). As reported recently, Ni can be dissolved from the surface of Pt-Ni allo[y] nanostructures while dispersed in nonpolar solvents such as hexane and chloroform.[15] Clean Pt surface was furth[er] supported by the CV during initial pre-cycling (Fig. S12). During the clean process, little change is observed in H_{upd} region whi[le] the H_{upd} rapidly increases in the data from commercial Pt_3Ni/C. Considering that increase of H_{upd} region was correlated from [Pt] exposure by electrochemical dealloying process,[16] the surface of our Pt-Ni nanostructures is almost fully covered with Pt atoms. On the other hand, according to energy dispersive x-ray spectroscopy (EDS) data, no significant dissolution of Ni fro[m] the nanostructures is observed after ADT (Fig. 2d, Fig. S13 and Table S3, ESI†). This shows the good stability our Pt-Ni bimetallic nanostructure under ORR condition.

In conclusion, we developed a facile synthesis of the urchin-like Pt-Ni nanostructures via simple one-pot process. The composition of Pt-Ni nanostructures is controlled by varying the molar ratio of the Pt and Ni precursors. Our nanostructures show 12.2 and 15.5 times higher mass and specific activity, respectively, than the commercial Pt/C nanoparticles for the ORR using $HClO_4$ electrolyte. Furthermore, under specific anion adsorption condition (H_2SO_4 electrolyte), our Pt_2Ni nanostructures exhibited 20.7 times higher specific activity than Pt. Also, we found that the urchin-like structure has better stability than spherical nanoparticles. These advantages of our nanostructures, including the higher activity, low specific anion adsorption, and long term stability, are explained in terms of their structural factors induced by the formation process.

Notes and references

This work was financially supported by the Research Center Program of the Institute for Basic Science (IBS) in Korea (Project Code: IBS-R006-D1 and IBS-R006-G1).

1 (*a*) R. O'Hayre, S. W. Cha, W. Colella and F. B. Printz, *Fuel Cell Fundamentals*, John Wiley & Sons, New Jersey, 2006. (*b*) W. Vielstich, A. Lamm and H. A. Gasteiger, *Handbook of Fuel Cells-Fundamentals*, Technology and Applications; Wiley & Sons, U.K., 2003.

2 EG&G Technical Services, *Fuel cell handbook* 7th ed., Parsons Inc., 2004.

3 (*a*) N. M. Marković, T. J. Schmidt, V. Stamenković and P. N. Ross, *Fuel Cells*, 2001, **1**, 105-116. (*b*) E. J. Antolini, *Mater. Sci.*, 2003, **38**, 2995-3005. (*c*) Z. Peng and H. Yang, *Nano Today*, 2009, **4**, 143-164. (*d*) N. Jung, D. Y. Chung, J. Ryu, S. J. Yoo and Y.-E. Sung, *Nano Today*, 2014, **9**, 433-456.

4 (*a*) C. Wang, H. Daimon, Y. Lee, J. Kim and S. Sun, *J. Am. Chem. Soc.*, 2007, **129**, 6974-6975. (*b*) C. Wang, H. Daimon, T. Onodera, T. Koda and S. Sun, *Angew. Chem., Int. Ed.*, 2008, **47**, 3588-3591.

5 (*a*) V. R. Stamenkovic, B. Fowler, B. S. Mun, G. Wang, P. N. Ross, C. A. Lucas and N. M. Markovic, *Science*, 2007, **315**, 493-497. (*b*) S.-I. Choi, S. Xie, M. Shao, J. H. Odell, N. Lu, H.-C. Peng, L. Protsailo, S. Guerrero, J. Park, X. Xia, J. Wang, M. J. Kim and Y. Xia, *Nano Lett.*, 2013, **13**, 3420-3425. (*c*) J. Zhang, H. Yang, J. Fang and S. Zou, *Nano Lett.*, 2010, **10**, 638-644. (*d*) J. Wu, A. Gross and H. Yang, *Nano Lett.*, 2011, **11**, 798-802. (*e*) C. Cui, L. Gan, H.-H. Li, S.-H. Yu, M. Heggen and P. Strasser, *Nano Lett.*, 2012, **12**, 5885-5889. (*f*) M. K. Carpenter, T. E. Moylan, R. S. Kukreja, M. H. Atwan and M. M. Tessema, *J. Am. Chem. Soc.*, 2012, **134**, 8535-8542. (*g*) D.-F. Zhang, J. Li, J.-X. Kang, T.-W. Chen, Y. Zhang, L.-L. Wang and L. Guo, *CrystEngComm*, 2014, **16**, 5331-5337. (h) J. Wu, J. Zhang, Z. Peng, S. Yang, F. T. Wagner and H. Yang, *J. Am. Chem. Soc.*, 2010, **132**, 4984-4985. (i) J. Wu, L. Qi, H. You, A. Gross, J. Li and H. Yang, *J. Am. Chem. Soc.*, 2012, **134**, 11880-11883. (j) C. Wang, M. Chi, G. Wang, D. van der Vliet, D. Li, K. More, H.-H. Wang, J. A. Schlueter, N. M. Markovic and V. R. Stamenkovic, *Adv. Funct. Mater.*, 2011, **21**, 147-152. (*k*) T.-Y. Jeon, S. J. Yoo, Y.-H. Cho, K.-S. Lee, S. H. Kang and Y.-E. Sung, *J. Phys. Chem. C*, 2009, **113**, 19732-19739. (*l*) D. Wang, H. L. Xin, R. Hovden, H. Wang, Y. Yu, D. A. Muller, F. J. DiSalvo and H. D. Abruña, *Nat. Mater.*, 2013, **12**, 81-87. (*m*) S. Chen, P. J. Ferreira, W. Sheng, N. Yabuuchi, L. F. Allard and Y. Shao-Horn, *J. Am. Chem. Soc.*, 2008, **130**, 13818-13819. (n) J. Gu, G. Lan, Y. Jiang, Y. Xu, W. Zhu, C. Jin and Y. Zhang, *Nano Res.*, 2015, **8**, 1480-1496.

6 (*a*) B. Lim, M. J. Jiang, P. H. C. Camargo, E. C. Cho, J. Tao, X. M. Lu, Y. M. Zhu and Y. N. Xia, *Science*, 2009, **324**, 1302-1305. (*b*) X. Q. Huang, E. B. Zhu, Y. Chen, Y. J. Li, C. Y. Chiu, Y. X. Xu, Z. Y. Lin, X. Duan and Y. Huang, *Adv. Mater.*, 2013, **25**, 2974-2979.. (*c*) D.-S. Kim, C. Kim, J.-K. Kim, J.-H. Kim, H.-H. Chun, H. Lee and Y.-T. Kim, *J. Catal.*, 2012, **291**, 69-78.

7 (*a*) J. Park, K. An, Y. Hwang, J.-G. Park, H.-J. Noh, J.-Y. Kim, J.-H. Park, N.-M. Hwang and T. Hyeon, *Nat. Mater.*, 2004, **3**, 891-895. (*b*) K. An, N. Lee, J. Park, S. C. Kim, Y. Hwang, J.-G. Park, J.-Y. Kim, J.-H. Park, M. J. Han, J. Yu and T. Hyeon, *J. Am. Chem. Soc.*, 2006, **128**, 9753-9760. (*c*) J. Park, J. Joo, S. G. Kwon, Y. Jang and T. Hyeon, *Angew. Chem., Int. Ed.*, 2007, **46**, 4630-4660. (d) S. G. Kwon and T. Hyeon, *Small*, 2011, **7**, 2685-2702.

8 (*a*) J. D. S. Newman and G. J. Blanchard, *Langmuir*, 2006, **22**, 5882-5887. (*b*) L. C. Ciacchi, W. Pompe and A. D. Vita, *J. Phys. Chem. B*, 2003, **107**, 1755-1764. (*c*) E. Herrero, L. J. Buller and H. D. Abruña, *Chem. Rev.*, 2001, **101**, 1897-1930. (d) M. Chatenet, R. Faure and Y. Soldo-Olivier, *J. Electroanal. Chem.*, 2005, **580**, 275-283.

9 J. Gu, Y.-W. Zhang and F. Tao, *Chem. Soc. Rev.*, 2012, **41**, 80[illegible] 8065.

10 (*a*) Y. S. Kim, S. H. Jeon, A. Bostwick, E. Rotenberg, P. N. Ros[illegible] V. R. Stamenkovic, N. M. Markovic, T. W. Noh, S. Han and B. S. Mun, *Adv. Energy Mater.*, 2013, **3**, 1257-1261. (*b*) S. J. Hwang, S. K. Kim, J. G. Lee, S. C. Lee, J. H. Jang, P. Kim, T. H. Lim, Y.-[illegible] Sung and S. J. Yoo, *J. Am. Chem. Soc.*, 2012, **134**, 19508-19511.

11 N. Markovic, H. Gasteiger and P. N. Ross, *J. Electrochem. Soc.*, 1997, **144**, 1591-1597.

12 (a) R. Subbaraman, D. Strmcnik, V. Stamenkovic and N. Markovic, *J. Phys. Chem. C*, 2010, **114**, 8414-8422. (b) R. Subbaraman, D. Strmcnik, A. Paulikas, V. Stamenkovic and N. Markovic, *ChemPhysChem*, 2010, **11**, 2825-2833. (c) J. Tymoczko, F. Calle-Vallejo, V. Colic, M. T. M. Koper, W. Schuhmann and A. S. Bandarenka, *ACS Catal.*, 2014, **4**, 3772-3778.

13 (*a*) N. M. Markovic, H. A. Gasteiger and P. N. Ross, *J. Phys. Chem.*, 1995, **99**, 3411-3415. (*b*) J. Mostany, E. Herrero, J. M. Feliu and J. Lipkowski, *J. Phys. Chem. B*, 2002, **106**, 1278[illegible] 12796. (*c*) C. M. Sánchez-Sánchez, J. Solla-Gullón, F. J. Vidal-Iglesias, A. Aldaz, V. Montiel and E. Herrero, *J. Am. Chem. Soc.*, 2010, **132**, 5622-5624. (*d*) Q. S. Chen, F. J. Vidal-Iglesias, J. Solla-Gullón, S. G. Sun and J. M. Feliu, *Chem. Sci.*, 2012, **3**, [illegible] 147.

14 (a) D. -S. Kim, C. Kim, J. –K. Kim, J. –H. Kim, H. –H. Chun. H. Lee and Y. –T. Kim, *J. Catal.*, 2012, **291**, 69-78. (b) S. Sun, G. Zhang, D. Geng, Y. Chen, R. Li, M. Cai and X. Sun, *Angew. Chem. Int. Ed.*, 2011, **50**, 422-426. (c) J. –N. Zheng, L. –L. He, C. Chen, A. –J. Wang, K. –F. Ma and J. –J. Feng, *J. Power Sources*, 201[illegible] **268**, 744-751.

15 C. Chen, Y. Kang, Z. Huo, Z. Zhu, W. Huang, H.L. Xin, J.D. Snyder, D. Li, J.A. Herron, M. Mavrikakis, M. Chi, K.L. More, Y. Li, N.M. Markovic, G.A. Somorjai, P. Yang and V.R. Stamenkovic, *Science*, 2014, **343**, 1339-1343.

16 D. Wang, Y. Yu, J. Zhu, S. Liu, D.A. Muller and H.D. Abruña, *Nano Lett.*, 2015, **15**, 1343-1348.